Source history of the 1905 great Mongolian earthquakes (Tsetserleg, Bolnay)

Antoine Schlupp, Armando Cisternas

Geophys. J. Int. (2007) **169,** 1115–1131 doi: 10.1111/j.1365-246X.2007.03323.x

Source history of the 1905 great Mongolian earthquakes (Tsetserleg, Bolnay)

Antoine Schlupp and Armando Cisternas

Institut de Physique du Globe, 5 rue René Descartes, 67084 *Strasbourg, France. E-mail: antoine.schlupp@eost.u-strasbg.fr*

Accepted 2006 December 6. Received 2006 December 5; in original form 2005 November 18

SUMMARY

Two great Mongolian earthquakes, Tsetserleg and Bolnay, occurred on 1905 July 9 and 23. We determined the source history of these events using body waveform inversion. The Tsetserleg rupture (azimuth N60°) correspond to a N60° oriented branch of the long EW oriented Bolnay fault.

Historical seismograms recorded by Wiechert instruments are digitized and corrected for the geometrical deformation due to the recording system. We use predictive filters to recover the signals lost at the minute marks.

The total rupture length for the Tsetserleg earthquake may reach up to 190 km, in order to explain the width of the recorded body waves. This implies adding 60 km to the previously mapped fault. The rupture propagation is mainly eastward. It starts at the southwest of the central subsegment, showing a left lateral strike-slip with a reverse component. The total duration of the modelled source function is 65 s. The seismic moment deduced from the inversion is 10^{21} N m, giving a magnitude $M_w = 8$.

The nucleation of the Bolnay earthquake was at the intersection between the main fault (375 km left lateral strike-slip) and the Teregtiin fault (N160°, 80 km long right lateral strike-slip with a vertical component near the main fault). The rupture was bilateral along the main fault: 100 km to the west and 275 km to east. It also propagated 80 km to the southeast along the Teregtiin fault. The source duration was 115 s. The moment magnitude Mw varies between 8.3 and 8.5.

The nucleation and rupture depths remain uncertain. We tested three cases: (1) nucleation and rupture depth limited to the seismogenic zone; (2) nucleation in the seismogenic zone and rupture propagation going to the base of the crust and (3) nucleation within the crust–upper mantle interface and rupture propagation within the upper mantle.

Key words: Mongolia, rupture progagation, source time functions, tectonics, waveform analysis.

INTRODUCTION

Four of the 20 intracontinental earthquakes with magnitude larger then 8, which occurred during the XXth century, took place in the region of Mongolia (Richter 1958; Kanamori 1977; Okal 1977; Khil'ko *et al.* 1985), (Fig. 1). Two of them are particularly interesting (Fig. 2), the Tsetserleg event of 1905 July 9 at 9 hr 40 m UT [$M_w = 8.4$ (Kanamori 1977), $M_s = 7.9$ (Okal 1977)] and the Bolnay earthquake of 1905 July 23 at 2 hr 47 m UT [$M = 8.7$ (Richter 1958), $M_w = 8.4$ (Kanamori 1977); $M = 8.2$ (Khil'ko *et al.* 1985)] which is one of the largest known events within a continental region. Since the available data were limited to Europe, the azimuths 'epicentre to station' are very similar. Nevertheless, we have a good knowledge of the surface ruptures. They were mapped a few months after the events (Voznesenskii & Dorogostaiskii 1914). Their observations were completed by Aprodov (1960), Khil'ko *et al.* (1985) and Baljinnyam *et al.* (1993).

The first segment, known as Tsetserleg, is oriented N60°E and has been mapped over 130 km. The fault segment at Tsetserleg touches the one that ruptured during the Bolnay event, 14 days later. A left lateral movement characterizes its northeastern part with a reverse component dipping to the northwest. Near the intersection with the Bolnay fault, the movement becomes purely strike-slip. The average displacement is 2 ± 0.5 m for the horizontal component and about 1 m for the vertical component. The segments activated during the Bolnay earthquake are clearly visible on the satellite images, whereas those of the Tsetserleg event are more difficult to identify (Okal 1977). The EW oriented Bolnay rupture is characterized by an almost pure left lateral strike-slip over a length of 375 km (all ruptured segments give a length of 455 km). The average horizontal displacements are of 10 ± 2 m over 200 km, 8 ± 2 m over 100 km and 5 ± 2 m over 75 km (Baljinnyam *et al.* 1993). Two other smaller segments were activated on 1905 July 23. The Teregtiin segment oriented N160°, is characterized by a

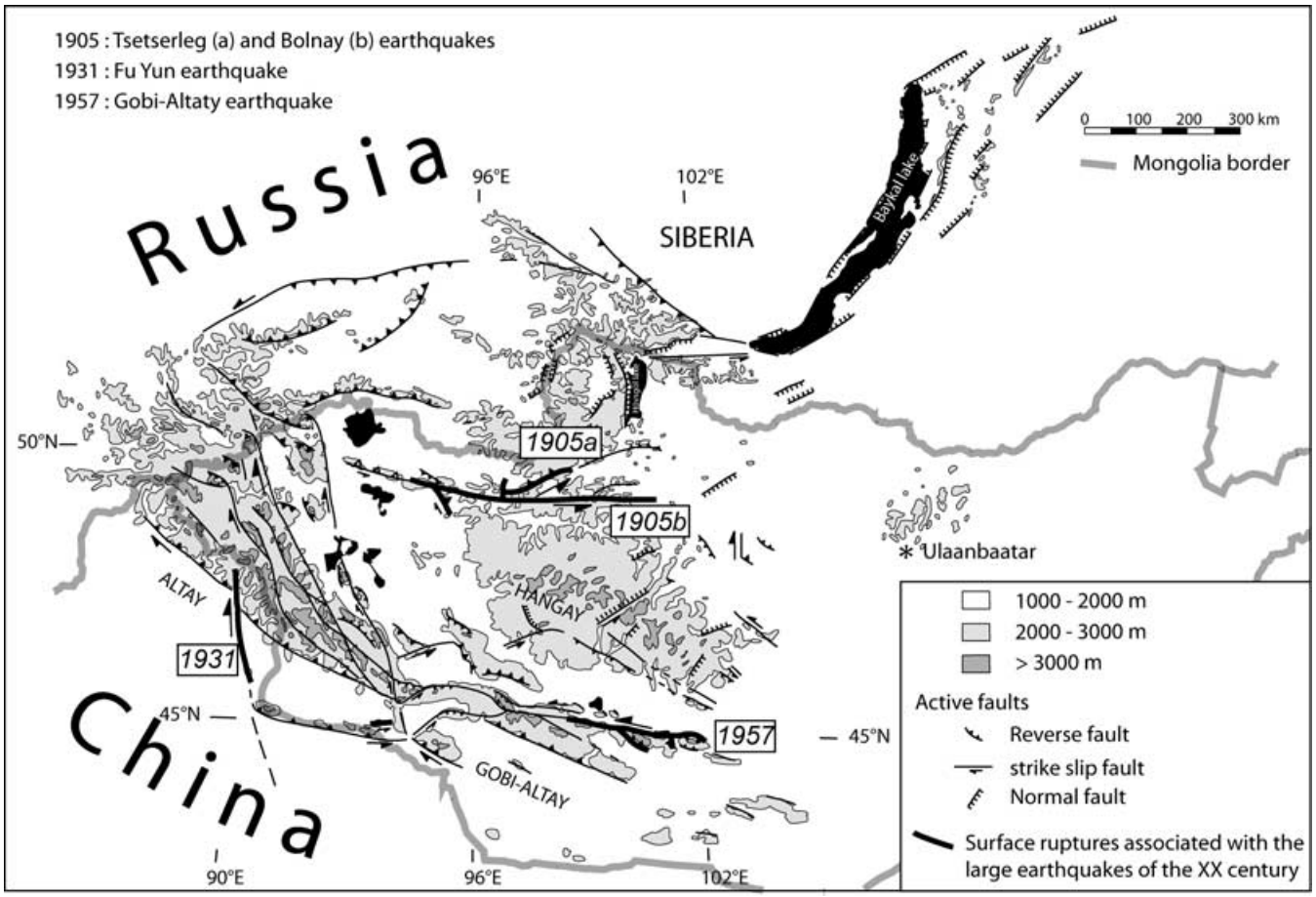

Figure 1. Main active faults in Mongolia and the large earthquakes of the XX century (after Schlupp 1996).

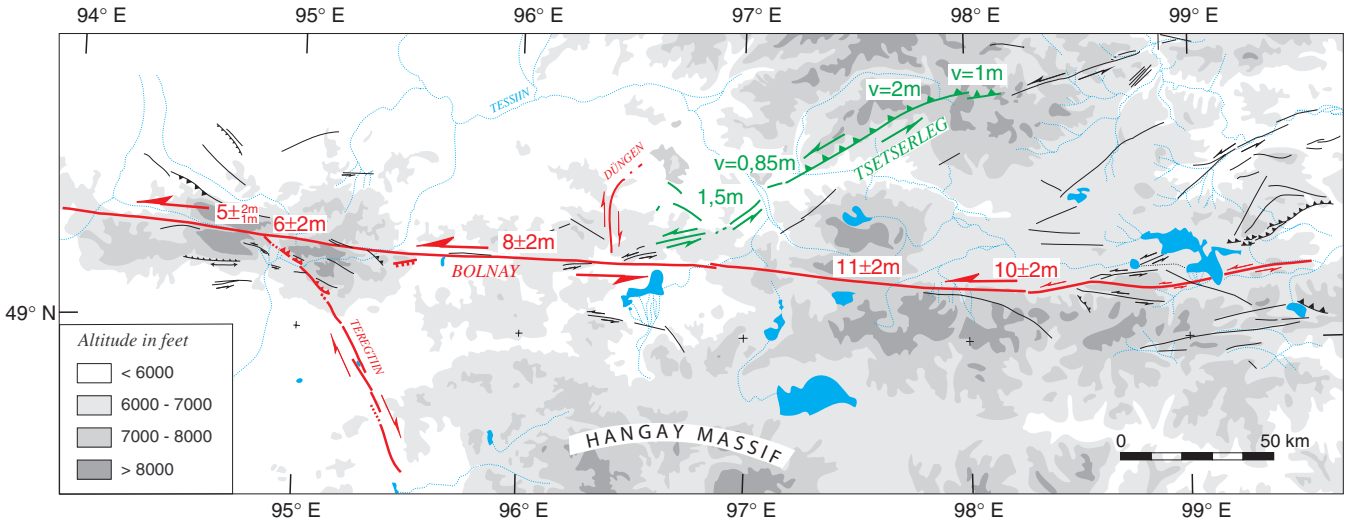

Figure 2. Surface ruptures associated with the Tsetserleg earthquake (1905 July 9, in green) and the Bolnay earthquake (1905 July 23, in red). Active faults in Hangay region are in black.

right lateral motion at the south west of the Bolnay fault. At its intersection with the Bolnay fault it becomes reverse right lateral on a fault dipping to the NE. Other branch is called the Düngen fault, located to the north of the Bolnay rupture, near its centre, and close to the junction of Bolnay and Tsetserleg. Voznesenskii & Dorogostaiskii (1914), Voznesenskii (1962) and Khil'ko *et al.* (1985) reported a right lateral component on a subvertical NS oriented fault.

These events where studied by using Love G1 waves recorded at Göttingen (Okal 1977). The recent evolution of methods and tools allow us to extract more information from the 1905 seismograms: Is the Tsetserleg segment associated to the July 9 event? What is

their source history? What are the focal depth, rupture length and width, or seismic moment? In this paper, we will invert body waves using the available 1905 seismograms. The first part of the paper concerns the instrumental corrections. The second part is devoted to the source history of the events.

CORRECTION OF THE WIECHERT SEISMOGRAMS BEFORE BODY WAVEFORM INVERSION

In 1905 there were about a hundred seismic stations operating around the world (Wood 1921). We could use only four stations (Jena, Göttingen, Uppsala and Strasbourg) because we selected the distance (30° to 90°), the recording geometry (no circular recording as Ewing), damped seismometers (we did not use the Milne seismogram) and the largest possible azimuth distribution. All selected instruments were Wiechert seismographs with a mass of 1000 kg (Wiechert 1903, 1904). Table 1 shows the station characteristics.

When looking for surface waves of large earthquakes, we found that the Wiechert instrument was saturated, or that its recording needle was broken. In fact, we did not find any record of surface waves other than the one used by Okal (1977). However, the body waves were in general clearly recorded, except for one horizontal component of the Bolnay earthquake which was lost at Strasbourg.

The horizontal component works as a reversed pendulum with a stationary mass of approximately 1000 kg. On the other hand, there were no Wiechert vertical components before 1906. The same pendulum records the two horizontal components of the ground shaking, and may produce a coupling between them. For our study, we consider it as negligible. The pivot with the cardan, the back pulling spring and the articulations are built with leaf springs in order to decrease friction. The amplification adjustment is mechanical, uses connecting rod and lever, and it is separated for each component. Its value generally varies from 150 to 250 for the 1000 kg Wiechert. The natural period, partially adjustable, varies between 9 and 15 s. The damping, by forced air circulation between a cylinder and a piston, is about $\varepsilon = 4 \pm 1$. The Wiechert works linearly for small oscillations.

We have compared for each station the amplification curves without, and with, solid friction using Reid (1910, 1925) approximation which corresponds to an approximate harmonic representation of the non-linear response of the seismometer. The solid friction reduces the amplification factor functions of the natural period of the instrument, the signal frequency and the recorded amplitude. This representation is not valid at the beginning of the signal. We observe that: solid friction becomes very important for small amplitudes (less than 6 mm for Göttingen) even at periods (about 9 s) smaller than the natural period (about 14 s). For periods less than half the natural period of the pendulum, the impact of solid friction becomes very small. The decrease of amplitude is less than 10 per cent for values larger than 21 mm. Since the observed signal amplitudes are about 20–30 mm, we consider that the amplitude decrease is less than 10 per cent. The problem being non-linear, we cannot quantify exactly the effect of friction. Nevertheless, the important mass of the Wiechert (1000 kg) limits its impact.

The signal was recorded on smoked paper. The paper was placed on a cylinder of 6 cm in diameter, which is coupled to a driving system, and stretched by an aluminium cylinder at its bottom. It moves at a velocity that can be adapted between 10 and 30 mm min^{-1}. The cylinder and the paper are laterally displaced at a rate of 4.5 mm hr^{-1} thus producing a helicoidally trace. The needle is placed at the end of an arm moving in any direction through a cardan system and, in absence of motion, it should be at the vertical of the axis of the driving cylinder. Thus, the needle movement corresponds to the intersection between a cylinder and a sphere. This geometry induces a curved deformation of the signal (Fig. 3). In practice, the equilibrium position of the needle arm may not be perpendicular to the driving cylinder axis. This adds an inclination to the previous deformations of the signal (Fig. 3). The value of the arm shift is not measured during the recording, and it must be deduced. Moreover, the two needles are lifted each minute during a few seconds.

Table 1. Station parameters for Tsetserleg and Bolnay earthquakes, 1905 July 9 and 23.

Station name	B_az	Coordinate	N–S component				E–W component			
Inst. year.	Dist.	of the station	To (s)	*V*	ε β	*r* (mm)	To (s)	V	ε	*r* (mm)
Station parameters for Tsetserleg earthquake, 1905 July 9										
Göttingen[b]	55.4°	51°32′47″N	14	164	**4.9**	1.6	14.5	179	4.9	1.7
1901	52.3 °	9°57′51″E			*0.45*					
Uppsala[c]	66.3°	59°51′30″N	9.8	181	**4.7**	NC	10.8	185	4. 4	NC
1904	44.5°	17°37′36″E			*0.44*					
Strasbourg[a]	52.5°	48°35′05″N	10.15	248	**3.44**	2.55	10.1	202.5	3.4	1.08
1903	55.2°	7°45′57″E	+0.55	± 2	**+0.56**	+1.15	+0.8	±1.5	+0.1	+2.42
			−1.15		**−0.54**	−1.55	−1.1		−2.8	−0.48
					0.37					
					0.037					
					−0.045					
Station parameters for the Bolnay earthquake, 1905 July 23										
Göttingen[b]	56.1°	51°32′47″N	14	164	**4.9**	1. 6	14.4	179	4.8	1.7
1901	51.9°	9°57′51″E			*0.45*					
Jena[d]	56.5°	50°56′07″N	11.2	183	**4.9**	0. 5	11.6	171	4.9	0. 7
1903	51.4°	11°35′00″E			*0.45*					
Uppsala[c]	67.2°	59°51′30″N	9.8	181	**4.7**	NC	10.8	185	4.4	NC
1904	44.1°	17°37′36″E			*0.44*					

V = amplification; ε = damping coefficient, β = damping constant; r = solid friction; NC = not communicated; Inst. year. = Installation year of the Wiechert seismograph; B_az = backazimuth in degrees; Dist = distance station source in degrees. [a]Variation of the linearly extrapolated values between June and October 1905 (Mainka 1910). [b]Values written on the seismograms. [c]Values obtained from the response curves of the seismograms. [d]Values measured on March 31, 1905. To = natural period of the pendulum.

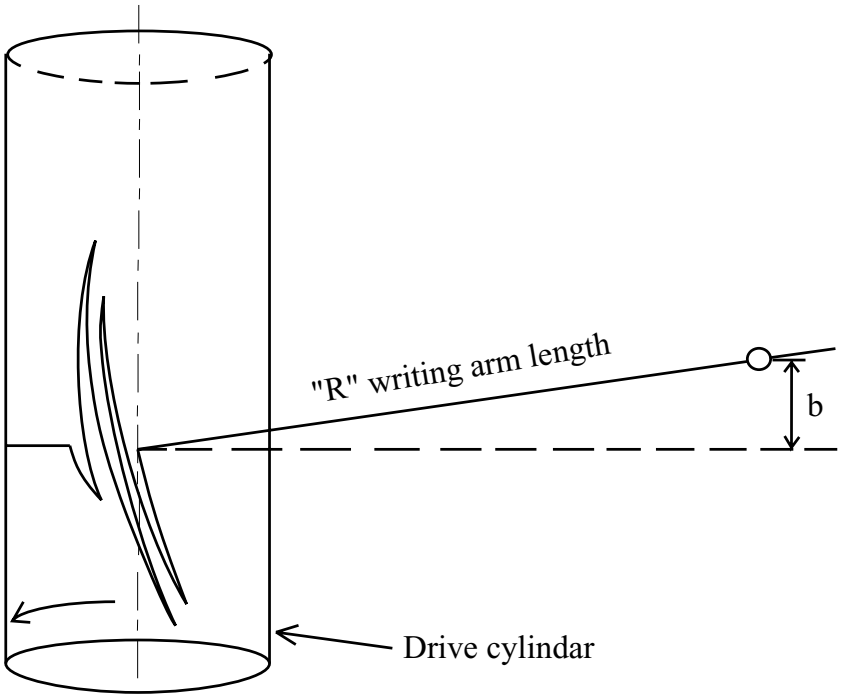

Figure 3. Geometrical deformations induced by the shift 'b' of the writing arm (after Cadek 1987).

Correction of data

Historical seismograms are being used more frequently now, due to the recent efforts to organize the collections, and to digitize the old records (Ferrari 2000; Michelini *et al.* 2005).

After scanning the records at high resolution, the original trace was precisely redrawn by using Adobe Illustrator. This manual step is irreplaceable because no automatic process can separate intersecting traces, despite the recent development of related software (Pintore *et al.* 2005). The trace is then transformed to a dense set of points, with coordinates (x_i, y_i). We obtained a few thousands points for about 200 s of signal.

Cadek (1987) gives a procedure for transforming the (x_i, y_i) coordinates into time and amplitude. To use it, it is necessary to know the radius of the cylinder, the length of the recording arm, and the distance from the axis of the rotating arm to the axis of the cylinder. Nevertheless, the shift 'b' of the axis of the arm with respect to the base line must be deduced directly from records. The deformations due to the shift 'b' are combined with those due to the whole geometry of the recording system. Therefore, we correct the data for all the deformations for different trial values of 'b', and then we choose the best 'b' value (lowest error). Within this procedure we considered the following criteria: (1) the signal must never go back in time; (2) upward time equal to downward time of signal and (3) The histogram of slope at 90° must be null.

The second criterion, (2), was used by Crouse & Matuschka (1983), who extrapolated the SEMOC methodology (Strong Earthquake Motion Centre, Japan) applied to SMAC accelerograms. They consider that the duration of the upward motion of the needle is equal to the downward one. We checked this postulate on modern seismograms. The case, in which both durations were equal, was rare. Indeed, this criterion produces artificial symmetry and is even more doubtful for surface waves, because it perturbs the dispersion.

The first, (1), and third procedures, (3), are the most reliable for estimating the 'b' shift.

Table 2. '**b**' values chosen for the geometrical correction of the data. The sign (-) is used when the writing arm is displaced to the north or the east.

Stations	1905 July 9		1905 July 23	
	EW	NS	EW	NS
Göttingen	−10 mm	−10 mm	−28 mm	−18 mm
Uppsala	−33 mm	−21 mm	−21 mm	−25 mm
Strasbourg	15 mm	9 mm	—	—
Jena	—	—	4 mm	28 mm

We deduced different 'b' values for each record with an uncertainty going from ±1 to ±3 mm (Table 2). The maximum uncertainty induces a time error of ±0.5 s at an amplitude of 30 mm. The variation in amplitude, due to the observed 'b' shift (maximum 33 mm), is less than 1 per cent for an arm length of 450 mm. Considering the amplitudes being analysed, these uncertainties are negligible.

The correction process continues with the combination of the NS and EW components in order to obtain the radial and transverse ones. In this case, a time shift between the components is unacceptable. The error is usually due to the imprecise clock used, or to variations of the rotation rate of the drive cylinder. This time drift can be linear, sinusoidal or complex. But also, when the arm is far from the base line during the minute mark, it will be lifted earlier and put down later, so that the minute mark gap becomes longer. Therefore, even though the timing mechanism is common for the two components, the beginning of their minute marks may be different. Therefore, we consider the centre of the minute mark gap as reference, and we have to precisely report the gap duration. The correction done independently for Jena and Göttingen shows a very good correlation (Fig. 4).

In the case of the Bolnay earthquake, the source duration is 150 s if we suppose a rupture velocity of 2.5 km s^{-1} and a unilateral rupture along the 375 km of the main fault. As 1Hz is a reasonable sampling for the digitization of low speed mechanical seismograph

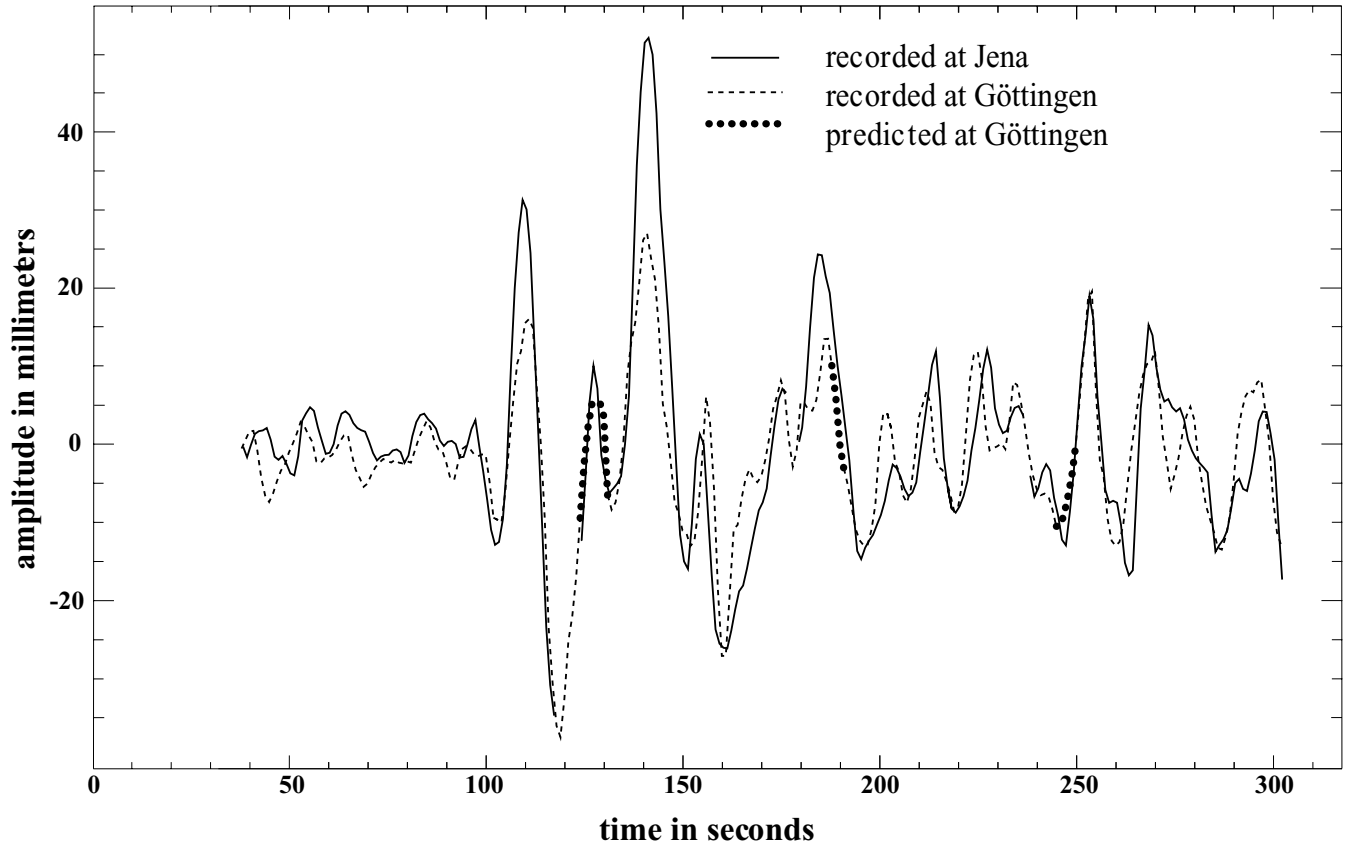

Figure 4. Comparison between the Göttingen and Jena '*S*' waveforms (Bolnay earthquake). The minute gaps at Göttingen are corrected by using predictive filters.

recordings and as we do not need higher frequencies, we sampled down the data to 1 second after applying a low pass filter (Butterworth with two poles) anti-aliasing at 2 s. The impact of the low pass filter is negligible for our study, as the record is made at teleseismic distances, and the natural period of our instruments is large, between 10 and 14 s.

Prediction of the signal lost during the minute mark

In order to fill the gaps at the minute marks, we applied a linear predictive filter (Press *et al.* 1992) in the increasing and decreasing time directions, using the signal before and after, respectively. Then, the two predicted values are averaged with weights given by the corresponding standard deviations. We verified the stability of the linear prediction by changing the length of the signal used in the filter. To evaluate the quality of the signal estimated in the gaps we profited from the fact that the available stations are close together, for example, Jena and Göttingen could be considered as a single station. Actually, we can compare Jena, Göttingen, Strasbourg and Uppsala since their epicentre-station azimuth varies less than 9° (Fig. 5).

When the first gap is preceded by only few seconds of signal, the quality of the prediction is limited. To minimize this problem, we applied the coefficients of the predictive filter obtained from the signal after the gap, to the signal before the gap.

To obtain good results using the linear predictive filter, the signal durations should be two to three times the natural period of the instrument. Notice that in our case, the predominant period is about the natural period of the available instrument (10–20 s).

We compared the final signal of the different stations, and we observed a good correlation of the results even though the data were corrected separately. For the Bolnay earthquake, we obtained *S* wave forms at Göttingen, Jena and Uppsala. The Jena station was not inverted, but compared to the synthetic (weight of 0 in the inversion), as the beginning of the predicted signal was poorly constrained, and since the station was near Göttingen. For the *P* waves, we obtained good signals at Jena and Uppsala. In the case of the Tsetserleg earthquake, we obtained well-constrained *S* waveforms at Göttingen and Uppsala, despite a poorly predicted signal for the first gap at Uppsala. In the case of *P* waves, we obtained the signal only at Uppsala. *P* and *S* wave are available at Strasbourg but they cannot be used in the inversion do to high solid friction. Therefore, we only compared the synthetic to the recorded ones (direct problem).

SH, *SV* and *P* components

For the inversion, we will use the *P*, *SV* and *SH* components of the signal which could be obtained by rotating the NS–EW traces and the *Z* component. As the vertical recording system did not exist that time, we used the values of emergence angles from the IASPEI91 model (Kennett 1991) in order to estimate the amplitudes of the *SV* and *P*. Within the working windows (140 to 150 s), we recorded the following waves: *S/pS/sS/SPn/PnS* which have a similar emergence angle (differences less than 0.5 degrees). Other arrivals during this period (*PKiKP/pPKiKP/sPKiKP*) have almost vertical emergence angles, and are quite invisible on the two horizontal components. The *PcP* arrives at more than 1 min for Göttingen and Jena and at

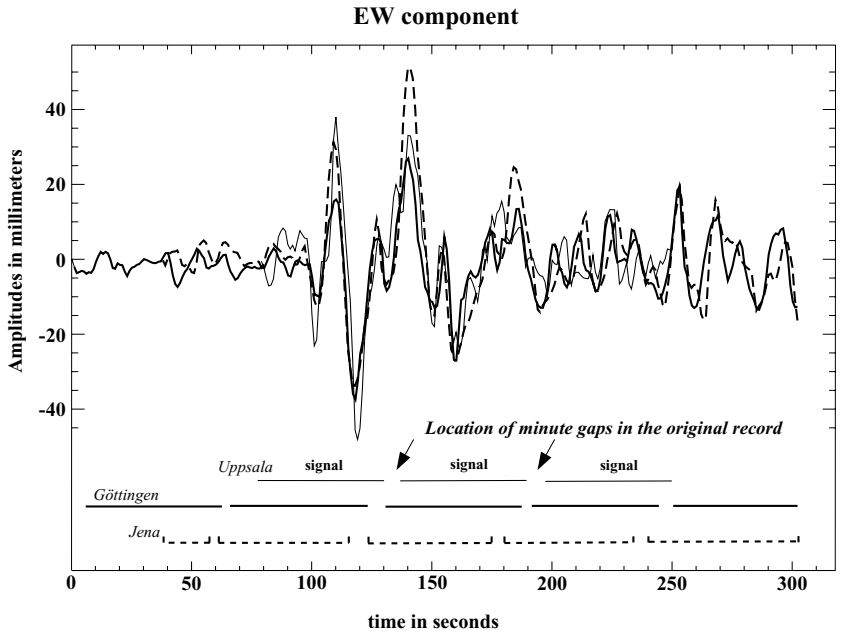

Figure 5. Comparison of the Bolnay '*S*' waveforms recorded at Jena, Uppsala and Göttingen after doing all corrections.

more than 1.5 min for Uppsala after the *P*. Then, for signal duration of 150 s, the use of a unique emergence angle is acceptable for the 1905 July 9 and 23 events except for the end of the *P* wave which could be affected by *PcP* with another emergence angle.

The *P* projection on the NS–EW plane and the emergence angle, allowed us to deduce the *P* waveform. We made the hypothesis that there was no *P/SV* conversion under the station that could modify the *P* waveform on the horizontal component, and then perturb the calculation of the *P* wave.

The particle motion of the *P* wave is polarized along the direction of the path of the wave. This allows us to verify the quality of the different corrections and rotations previously done on the data, as shown in Fig. 6.

BODY WAVEFORM INVERSION AND SOURCE HISTORY

All observed data has been normalized, using geometric and physical attenuation, to an epicentral distance of 40°, and then the instrumental amplification has been changed to 10 000. The t^* values considered are 1 s for *P* waves and 4 s for *S* waves. On the other hand, the synthetic seismograms have been convoluted with the transfer function of each instrument, before comparison with the observed records.

The Jena and Göttingen stations being very close, the recorded waveforms are very similar. The Uppsala, Göttingen and Jena stations were on granite, on limestone and on sandstone, respectively. The Strasbourg station was on thick sediments, and the recorded *S* waves were very low in amplitude and very noisy. *S* waves recorded at Strasbourg during the Tsetserleg earthquake, or at Jena during the Bolnay earthquake, were not inverted but only visually compared to synthetic seismograms. At the end, we used the waveforms recorded during the two earthquakes at Uppsala (*P*, *SH* and *SV*) and Göttingen (*SH* and *SV*), and the *P* waveform recorded at Jena during the Bolnay earthquake.

To determine the unknown parameters, we either inverted each of them, or we tested a set of '*a priori*' values, by using the Nabelek (1984) program. The parameters used in the source model are: azimuth, dip, slip on the fault, scalar seismic moment, depth of the nucleation, depth of the centroïd of each segment, amplitudes of the source time function and relative position of the different segments. The low number of available stations leads us to fix '*a priori*' values for the parameters. Therefore, we use all available information (observed surface ruptures, main regional tectonic features, crust and lithosphere structure, etc.) to constrain them. Finally, we invert first the less constrained parameters, and later on the remaining ones in order to verify the stability of the solution.

Rupture azimuths are well-known thanks to the observed surface ruptures (Fig. 2). In general, each segment measures several tenths of kilometres, and in the case of Bolnay, they are very linear. The fault dip is determined at the surface but it can vary with depth. We verified the consistency between the reliefs, the fault dip observed at surface, the main horizontal stress, and the GPS field (Calais *et al.* 2003).

We have no specific information about the nucleation depth. Usually it is restrained to the seismogenic layer. In the case of western Mongolia the crust is thick (50 ± 5 km; Villaseñor *et al.* 2001; Petit *et al.* 2002; Zorin *et al.* 2002). Then the seismogenic zone could be also thick, probably around 20–30 km. However, several earthquakes have been observed in the region at the base of the crust, down to 50 km (Chen & Molnar 1983; Nelson *et al.* 1987; Chen 1988; Déverchère *et al.* 1991, 2001; Bayasgalan 1999). Therefore, we will test various nucleation depths between 17 and 55 km. The total depth of the Bolnay rupture must be equal or larger than the nucleation depth. We cannot reject the possibility that the rupture propagates down through the whole crust (50 ± 5 km), or even through a part of the lithosphere, which is about 100 km thick in this region (Villaseñor *et al.* 2001; Petit *et al.* 2002). Therefore, we allowed a freedom on the parameter 'rupture depth' from 20 to 100 km.

The local velocity model used was one simple half-space crustal model with $Vp = 6\ \mathrm{km\ s^{-1}}$ $Vs = 3.46\ \mathrm{km\ s^{-1}}$ density $= 2.75\ \mathrm{g\ cm^{-3}}$. We considered a thickness of 60 km at source to model the particular crust in Mongolia, between 50 and 60 km.

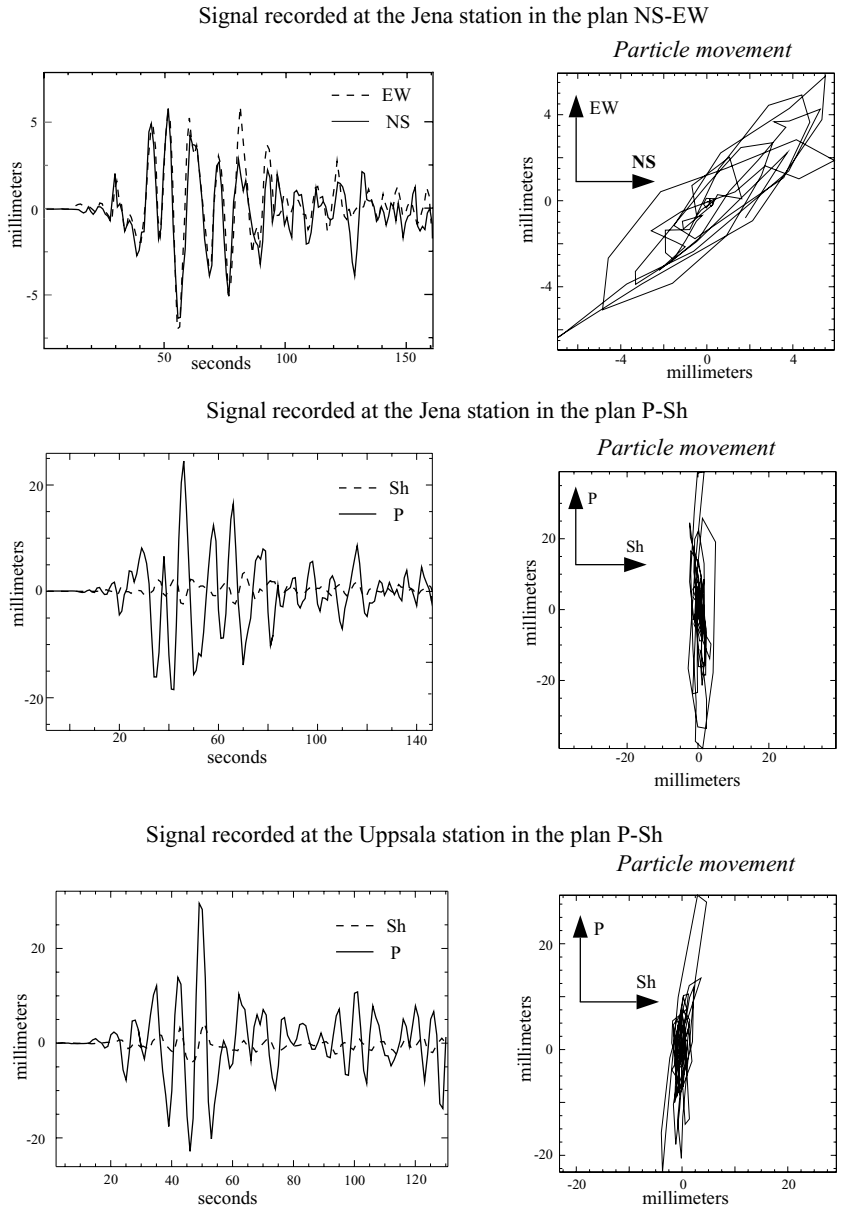

Figure 6. *P*-wave polarization—Bolnay 1905 earthquake.

The difference between the *P*- and *S*-wave duration resulting from the directivity effect is:

$$\Delta(S-P) = L\left(\frac{1}{\alpha} - \frac{1}{\beta}\right)\cos\psi,$$

where α and β are the *P*-and *S*-wave velocities at the source region, L the rupture length and ψ the angle between the rupture propagation and the epicentre-station directions. For the Uppsala station, the ψ angle relative to the main fault is either about 135° (propagation away from the station) or about 45° (propagation towards the station). The *P*-wave duration at Uppsala is about 75 s, whereas the *S*-wave duration is longer than 100 s (Fig. 7) which gives an angle $\psi > 123°$ according to the above formula. Therefore, we have to consider an eastward propagation along the Bolnay fault. This is in agreement with the result proposed by Okal (1977) by using the G1 surface waves recorded at Göttingen.

In the case of Tsetserleg, the angle ψ is about 75°. This implies a difference of less than 5 s between the length of *P*- and *S*-wave signals, too short to be observed with certainty.

If we consider the length of mapped surface ruptures (130 km) and the width of the body waveforms (70–80 s), we obtain a very low rupture velocity in the bilateral case. Hence we conclude that the rupture propagation of the Tsetserleg earthquake should be unilateral without being able to establish definitively the direction.

The time waveform is modelled by a set of triangular source elements (Nabelek 1984). The half-width of source element has been fixed at 4 or 5 s for the longest ruptures, and at 3 s for the shortest ones. This choice allows modelling the whole source and the highest frequencies observed in the signal. Beside the various parameters (azimuth, dip, slip on the fault, scalar seismic moment, depth of the nucleation, depth of the centroïd of each segment, amplitudes of the source time function and relative position of the different segments.),

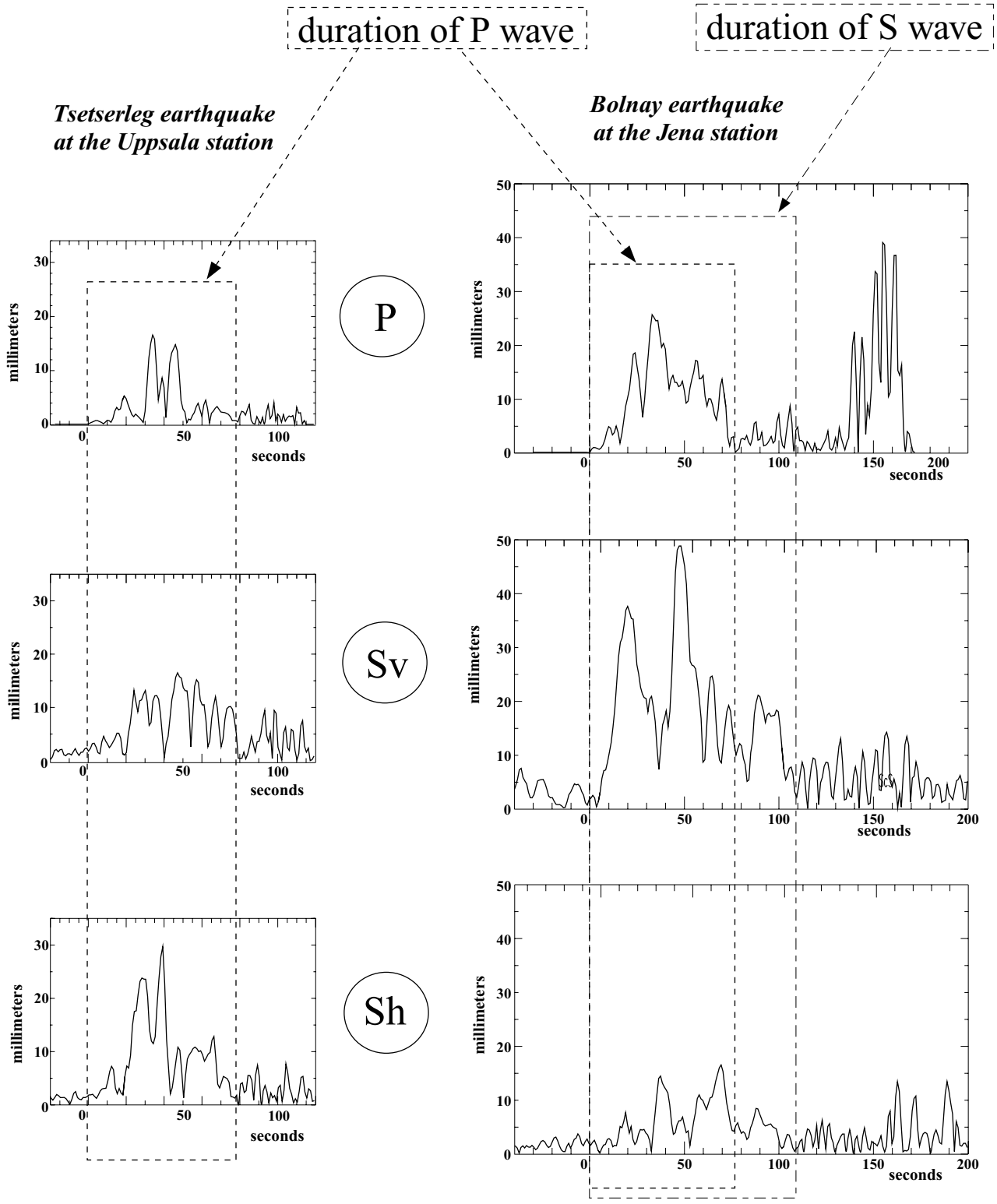

Figure 7. Signal envelope for the Tsetserleg and Bolnay 1905 earthquakes.

the most constrained parameters are the azimuth of the segments, the relative position of the segments and the slip angle. They are either fixed or inverted at the end, when the general result is consistent with the field data. We do not allow fault azimuth to vary more than 10° from the observed surface rupture and the slip or dip angles more than 20°. For the July 23 event, as the surface ruptures along the Bolnay fault are quite pure strike-slip and very linear, we allowed a freedom of only ±5° on the direction and ±6° on the slip angle permitting a maximal vertical movement of ±1 m. The amplitude of the source time function, the scalar seismic moment, the delay of each segment from the nucleation and the depth of the rupture were never fixed. The dip angle and the nucleation depth were most of the

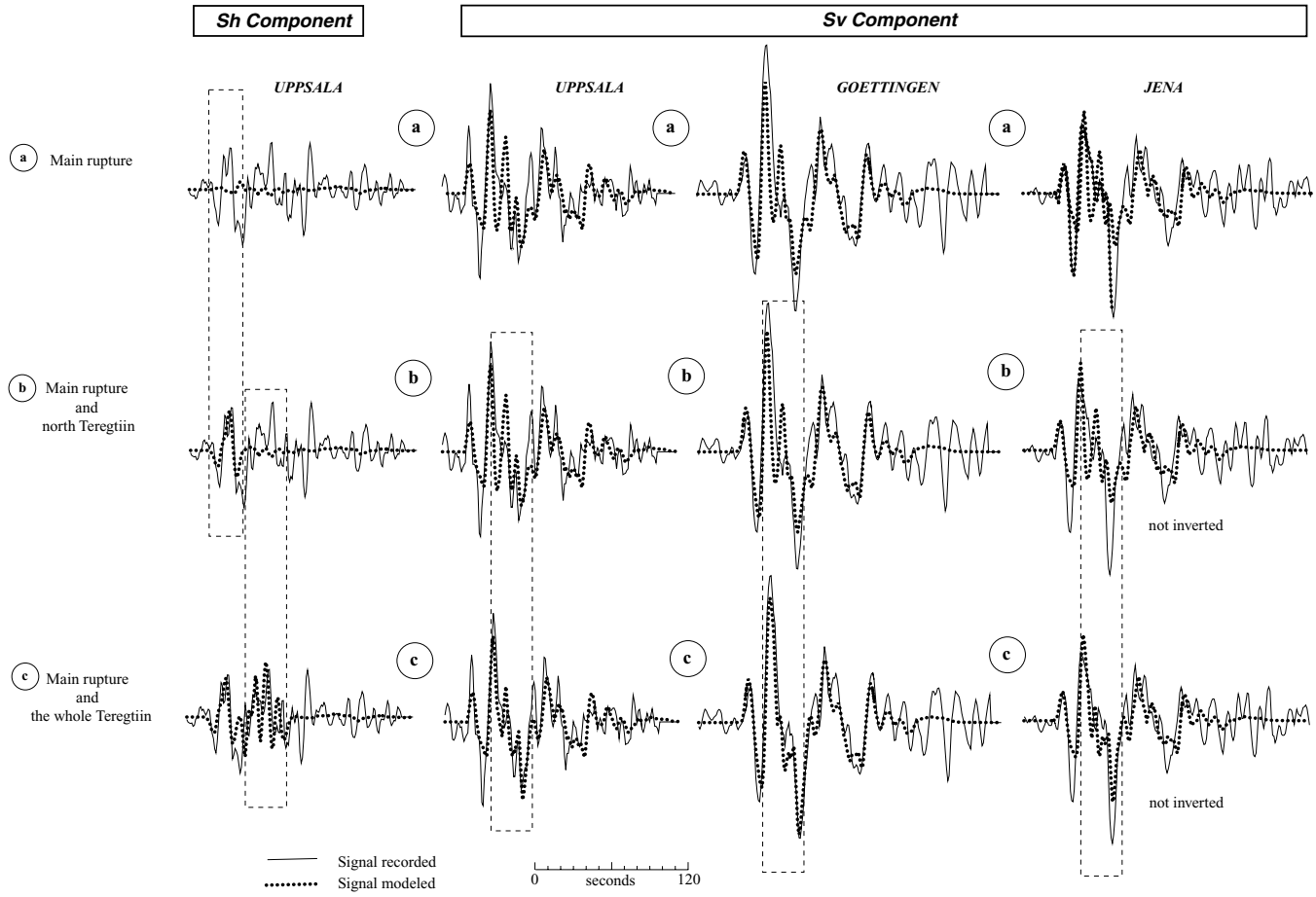

Figure 8. Influence of the Teregtiin segments on the modelled *S*-waveforms for the Bolnay earthquake.

time free. The depth of the rupture was always free. If the result of the inversion gives, for one parameter, values inconsistent with field information, we fixed them to stabilize the solution. This strategy is important as the result of the inversion depend strongly on the initial value of the parameters. The best results were obtained when we invert one to two parameters together, avoiding a rapid drift to aberrant solutions.

The Bolnay earthquake

We modelled first the Bolnay earthquake taking into account only the main fault, that is subvertical and oriented between N95° at the west and N90° to the east. Its length is about 375 km (Fig. 2). The surface ruptures show almost pure left lateral strike-slip with displacements between 8 ± 2 and 11 ± 2 m (Khil'ko *et al.* 1985; Baljinnyam *et al.* 1993). We saw before that the nucleation should be near the western part of the fault. In this way we obtain the most stable solution, and source duration consistent with the length of the fault, considering a rupture velocity of 2.5 km s^{-1}. Nevertheless, we cannot explain the amplitude or the *SH* polarity (Fig. 8a) because the stations are very near the nodal plan of the *SH* radiation. The tests with a change in the strike or a lower dip angle on the main rupture could not explain the amplitudes on *Sh*, *Sv* and *P* and became also inconsistent with the field observation. It appears then necessary to introduce another rupture mechanism at the beginning of the earthquake.

The Teregtiin fault has such an orientation that allows for important *SH* radiation in European stations. It was discovered only in 1958 by V. A. Aprodov & O. Namnandorg (Aprodov 1960) and studied in detail by Khil'ko *et al.* (1985). It has been associated to the 1905 July 23 earthquake because the scarp was fresh, and no other large event has been observed since. We can divide the Teregtiin fault into a north and south segment.

First, we introduced only the northern part of the Teregtiin rupture in the history of the source (Fig. 2). It is a reverse fault with a right lateral component, oriented N135° and dipping between 50° and 70° to the NE. We obtained an oblique displacement of 3.2 ± 1.1 m after Khil'ko *et al.* (1985) and Baljinnyam *et al.* (1993). Thus we can explain the form and the polarity of the beginning of the *SH* and the *P* waves (Fig. 8b). The Teregtiin segment must break first since numerous tests, placing it later in the history of the source, do not explain the beginning of *SH* and *P* waves. In conclusion, the nucleation must be near the junction of the Teregtiin and Bolnay faults, thus respecting a mainly eastward rupture propagation.

The southern part of the Teregtiin fault, oriented N160°, is a right lateral strike-slip segmented into several 'en echelon' ruptures along 60 km (Fig. 2). The displacements are of the order of 3 ± 1 m (Baljinnyam *et al.* 1993). The best fit is obtained if it starts 17 s after the nucleation. Adding this segment improves the *SH* and *SV* waveforms and gives higher amplitude on the *P* (Fig. 8c).

The Düngen complex segment, a NS right lateral strike-slip of about 1.5 ± 0.5 m, is at the junction between the ruptures of the July 9 and 23 earthquakes (Baljinnyam *et al.* 1993). The length is about 30 km. Starting at 22 s after the nucleation, it improves the *P*, *SH* and *SV* waveforms.

At the first step, we model a nucleation at 17 km depth, near the base of the seismogenic zone, and a rupture propagating down to 30 km, the schizosphere zone (Table 3a). The seismic moment suggested by Baljinnyam *et al.* (1993) ($M_o = 2.28 \pm 0.56 \times 10^{21}$ N m), which is deduced from the surface ruptures and a hypothetical rupture depth of 20 km, is much smaller than our solution ($M_o = 3.97 \pm 0.47 \times 10^{21}$ N m). Next, keeping the source nucleation at 17 km, we tested the propagation of the rupture in depth between 30 and 80 km (Table 3b). A value near 60 km gives the best results, and explains better the end of the recorded signal (Figs 9a and b). Third, assuming a crustal thickness of about 50 ± 5 km, we start with a nucleation near 45 km depth, and a rupture propagating down to 70 km (Table 3c). We inverted jointly these two parameters. The best total seismic moment, $M_o = 7.27 \pm 0.40 \times 10^{21}$ N m, is comparable to that estimated by Okal (1977) ($M_o = 5.5 \pm 2.5 \times 10^{21}$ N m).

Finally, the last solution, with the nucleation at 43 km depth and a rupture propagating down to 70 km, appears to be the most satisfactory. Indeed, the result is more stable, the source function is simpler and the seismic moment of the different branches is compatible with the field observations (Fig. 10a). Nevertheless, the natural period of the instruments, about 10–15 s, smoothes the signal and could favour the inversion of such large values of depth. If we fix the depth to moderate value, the waveforms are explained (Table 3a).

The *SH* component, at Goettingen and Uppsala, are poorly explained after 80 s. Considering only the known surface ruptures, it could not be modelled and neither another kind of wave arrivals, nor anisotropy can, up to now, explain it.

Tsetserleg earthquake

The Tsetserleg earthquake (1905 July 9) is not as well known as the one of Bolnay (1905 July 23). The access to the region of surface ruptures is difficult and, probably, some have not been seen (Voznesenskii & Dorogostaiskii 1914; Ilyin 1978; Khil'ko *et al.* 1985; Baljinnyam *et al.* 1993). Voznesenskii and Dorogostaiskii reached the region only 3 months after the earthquake, but they had enough information to say that the first event is associated to the Tsetserleg earthquake, and the second one to Bolnay.

The observed surface ruptures are about 130 km long. The northern 80 km correspond to a reverse left lateral fault oriented N 60° ± 10°, with a dip of 65° ± 10° to the NW, and a slip angle of 40° ± 20°. The southern 50 km are complex (Voznesenskii & Dorogostaiskii 1914), with subvertical left lateral strike-slip faults oriented N80° (Khil'ko *et al.* 1985).

The polarization of *S* waves at the Göttingen station changes from NW, at the beginning of the signal, to NE at the end, thus suggesting two different mechanisms. As the first results were very unstable, we decided to filter the high frequencies at 10 s by a two poles Butterworth low pass filter. We fixed the depth of the nucleation at 15 km, but allowed for a deep propagation of the rupture (Tables 4a and b).

Okal (1977) proposed a rupture propagating eastwards along a fault oriented EW. Hence, we first considered a nucleation at the southwestern end of the mapped surface ruptures, but the fit was poor. Then, we moved the nucleation to the southwestern end of the main fault with bilateral propagation (Fig. 11). Most of the waveforms were explained except for the *SV* wave, since its amplitude and length were underestimated.

Thus we needed a longer source history. We could not decrease the rupture velocity because the *P*- and *SH*-wave signals would be too long. An extension of the ruptures to the SW would imply that part of the Bolnay main fault broke, in contradiction with the previous wave modelling. Finally, we increased the fault length to the NE. Indeed, Kosmos satellite images show 80 km of active faults at the NE of the mapped surface ruptures. They are orientated N 80° ± 5° and they displace a river in a left lateral way (Table 4a).

By doing this, we obtained good results on most parts of the signal (Fig. 12). We could explain the strong amplitude on the *SV* and the rather small ones on the *SH* and *P* components. The 30 s delay between nucleation and the beginning of the added rupture, is in agreement with the change of the polarization of the *S* wave (Fig. 10b). Note that, despite adding this new structure, the end of the *S* wave is not completely explained. Okal (1977), using surface waves, proposed a total rupture length of about 200 ± 30 km with a rupture velocity of 3.5 km s^{-1}.

The total seismic moment is $1.06 \pm 0.05\ 10^{21}$ N m, giving $M_w = 7.95 \pm 0.02$. It implies about 2.4 m of displacement on the central segment and 2.6 m on the southwestern segment, in agreement with the 2.3 m considered by Baljinnyam *et al.* (1993). The added northeast segment should be associated with 7 m of left lateral strike-slip. Such important variations in slip between segments are possible and have been recently observed after the Kokoxili earthquake (Klinger *et al.* 2005) The previous magnitude published for the Tsetserleg event where: Okal 1977: $M_s = 7.9 \pm 0.2$; Kanamori 1977: $M_s = 8.25$; Abe 1981: $M_s = 8.4$; Baljinnyam *et al.* 1993 : $M_w = 7.5 \pm 0.1$.

We also tested rupture propagation to the west with the same segments. The obtained displacement on the central segment was 6.3 m, much higher than the 2 m observed on the field (Baljinnyam *et al.* 1993). Thus we favour the eastward propagation as proposed by Okal (1977).

Regional stress tensor

The Tsetserleg earthquake is located in a transition region where σ_1 goes from horizontal (south of Bolnay) to vertical (Baïkal rift). On one hand, we obtained the orientation of the main stress σ_1 at N30° using striations on the fault planes of the Bogd earthquake ($M_w = 8.1$ the 1957 December 4 associated to 250 km of surface rupture, with a main left lateral component, along the Gobi-Altay range; fig. 1; Khil'ko *et al.* 1985; Ritz *et al.* 1995; Schlupp 1996) and displacements associated to the Bolnay earthquake (1905 July 23). On the other hand, the Tsetserleg ruptures change in direction near the Tesiin River, where there are structures with EW extension and NS compression, suggesting a σ_1 oriented NS. For σ_1 horizontal and oriented NS, the best shape factor R is 0 ($\sigma_2 = \sigma_3$), meaning uniaxial compression (Armijo & Cisternas 1978). If we consider σ_1 oriented N30°, the best result is obtained for $R = -0.5$, corresponding to triaxial compression with σ_3 vertical. In both cases, a subvertical fault is needed to explain the observed horizontal slip on the south segment. The σ_1 direction makes an angle of 80° with the southern segment when σ_1 is oriented NS, and 60° when σ_1 is oriented N30°. This last solution is preferred because it favours shear along EW strike-slip faults.

Delouis *et al.* (2002) used fault plane solutions from the Tsetserleg–Bolnay sequence (Schlupp 1996) and two different procedures. They obtained a compressive tensor with σ_1 horizontal, oriented N41° to N49°. North of Tsetserleg they found a strike-slip tensor with σ_1 horizontal, oriented NS.

Thus, the region of the 1905 events consists of a transition zone with a rotation of σ_1 from N30°–49° to NS.

Table 3. The parameters of the solutions for the Bolnay earthquake (1905 July 23).

a: Nucleation in the seismogenic zone: Mo total = $(3.97 \pm 0.47).10^{21}$ N m = > $M_w = 8.34 \pm 0.04$

Depth of nucleation = 16.5 km	Strike (deg)	Dip (deg)	Slip (deg)	Distance (km)	Azimuth (deg)	Delay (seconds)	Depth of rupture (km)	Mo (N m)	Duration (sec)	Deduced slip (m)
Teregtiin north	312.0 ± 6.7	76.3 ± 4.1	143.6 ± 7.9	0	0	0	26.4 ± 2.1	(1.19 ± 0.13)e+20	18	3.3
West part of main fault	92.2 ± 1.2	85.5 ± 0.8	1.2 ± 0.9	12 NI	30 NI	1.43 ± 0.35	28.5 ± 0.4	(1.81 ± 0.11)e+21	60	14.1
Teregtiin south	337.0 ± 3.4	78.7 ± 2.4	177.3 ± 2.8	45 NI	153 NI	17.76 ± 0.15	30.4 ± 1.0	(3.46 ± 0.34)e+20	27	5.6
Düngen	0.0 ± NI	71.1 ± 1.9	157.9 ± 2.4	97 NI	84 NI	21.90 ± 0.15	23.0 ± 0.8	(1.54 ± 0.16)e+20	18	5.0
East part of main fault	88.4 ± 2.3	88.5 ± 2.4	6.4 ± 2.4	198 NI	90 NI	39.71 ± 0.26	36.7 ± 1.4	(1.54 ± 0.30)e+21	68	8.2

b: Nucleation in the seismogenic zone and propagation of the rupture in depth: Mo total = $(4.20 \pm 0.42).10^{21}$ Nm = > $M_w = 8.35 \pm 0.03$

Depth of nucleation = 17 km	Strike (deg)	Dip (deg)	Slip (deg)	Distance (km)	Azimuth (deg)	Delay (seconds)	Depth of rupture (km)	Mo (N m)	Duration (sec)	Deduced slip (m)
Teregtiin north	319.4 ± 5.6	76.7 ± 5.2	143.4 ± 5.4	0	0	0	60.7 ± 4.3	(1.12 ± 0.12)e+20	18	1.4
West part of main fault	92.2 NI	85.5 NI	1.2 NI	12 NI	30 NI	3.73 ± 0.31	60.7 ± 1.0	(2.25 ± 0.13)e+21	60	8.2
Teregtiin south	341.6 ± 1.6	79.0 ± 1.0	177.0 ± 1.3	45 NI	153 NI	18.61 ± 0.11	61.0 ± 1.0	(4.57 ± 0.31)e+20	27	3.7
Düngen	0.0 NI	71.1 NI	157.9 NI	97 NI	84 NI	24.60 ± 0.12	57.7 ± 1.2	(1.78 ± 0.17)e+20	18	2.3
East part of main fault	88.4 NI	88.5 NI	6.4 NI	198 NI	90 NI	35.98 ± 0.31	56.7 ± 2.4	(1.20 ± 0.23)e+21	68	4.1

c: Nucleation at the interface crust - mantle and propagation of the rupture in depth: Mo total = $(7.27 \pm 0.40).10^{21}$ N m = > $M_w = 8.51 \pm 0.02$

Depth of nucleation = 43 km	Strike (deg)	Dip (deg)	Slip (deg)	Distance (km)	Azimuth (deg)	Delay (seconds)	Depth of rupture (km)	Mo (N m)	Duration (sec)	Deduced slip (m)
Teregtiin north	315 NI	65 NI	135 NI	0	0	0	44.2 ± 2.5	(1.15 ± 0.10)e+20	18	1.9
West part of main fault	91.4 ± 1.0	88.0 ± 0.8	2.4 ± 0.8	23 ± 24	34 ± 17	5.37 ± 0.30	69.7 ± 0.9	(3.32 ± 0.12)e+21	60	10.6
Teregtiin south	339.9 ± 4.4	84.2 ± 0.9	174.9 ± 0.9	38 ± 10	139 ± 17	17.40 ± 0.43	27.6 ± 0.8	(4.08 ± 0.28)e+20	27	7.3
Düngen	0.0 NI	70.0 ± 2.4	154.0 ± 3.2	103 ± 15	79 ± 11	27.14 ± 0.14	70.7 ± 1.2	(1.24 ± 0.14)e+20	18	1.3
East part of main fault	88.3 ± 2.0	86.1 ± 1.0	5.4 ± 1.0	204 ± 20	86 ± 8	42.92 ± 0.26	78.8 ± 2.1	(3.38 ± 0.23)e+21	68	8.4

'NI' indicates that the parameter has not been inverted. The solution is stable for the seismic moment, the depth and the slip angle. The uncertainties on these values are significant. Nevertheless, for the other parameters, it was necessary to invert them one by one for each mechanism to get a solution close to the known parameters.

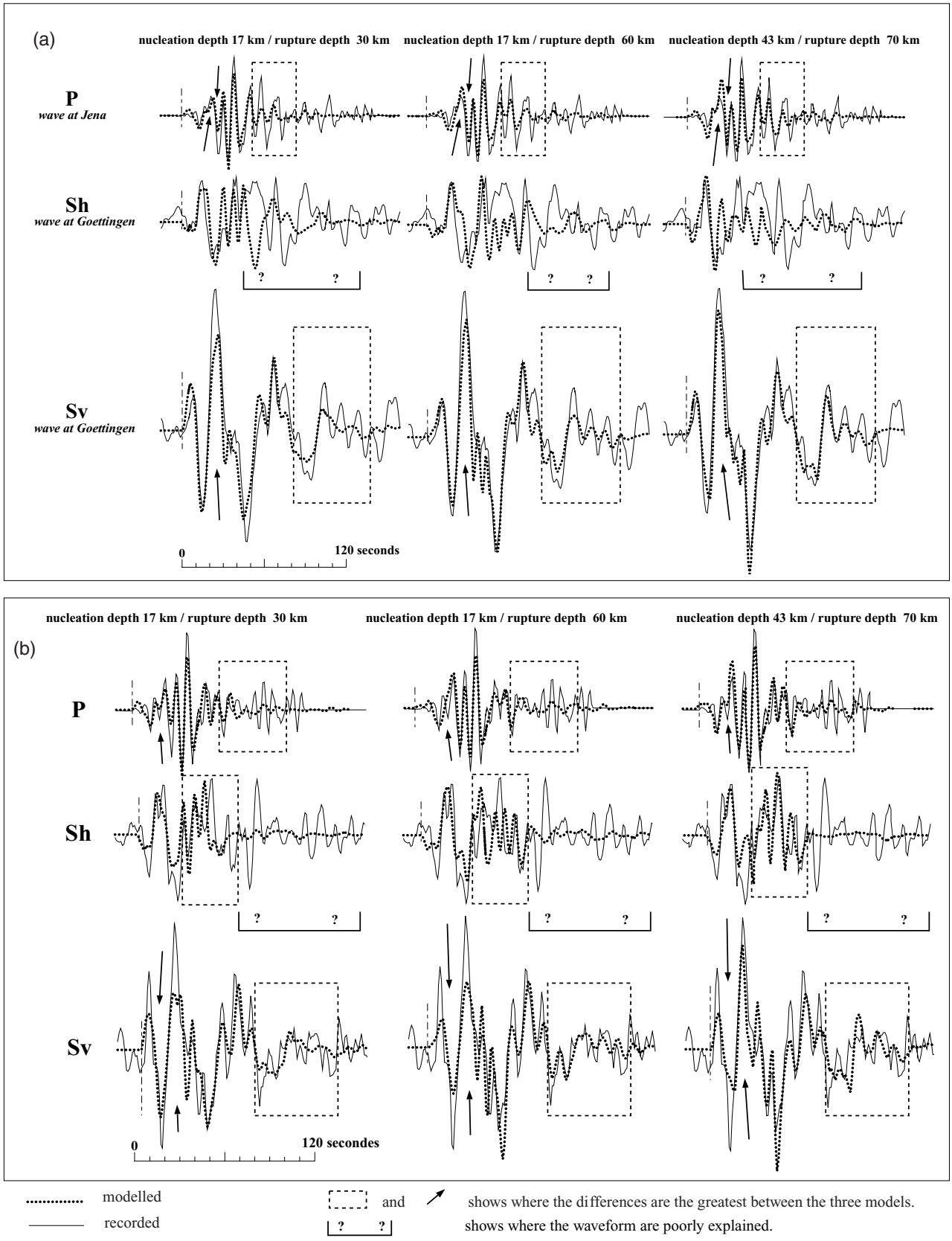

Figure 9. (a) Effect of the nucleation and rupture depths on the modelled body waveforms at Jena and Göttingen (Bolnay earthquake). (b) Effect of the nucleation and rupture depths on the modelled body waveforms at Uppsala (Bolnay earthquake).

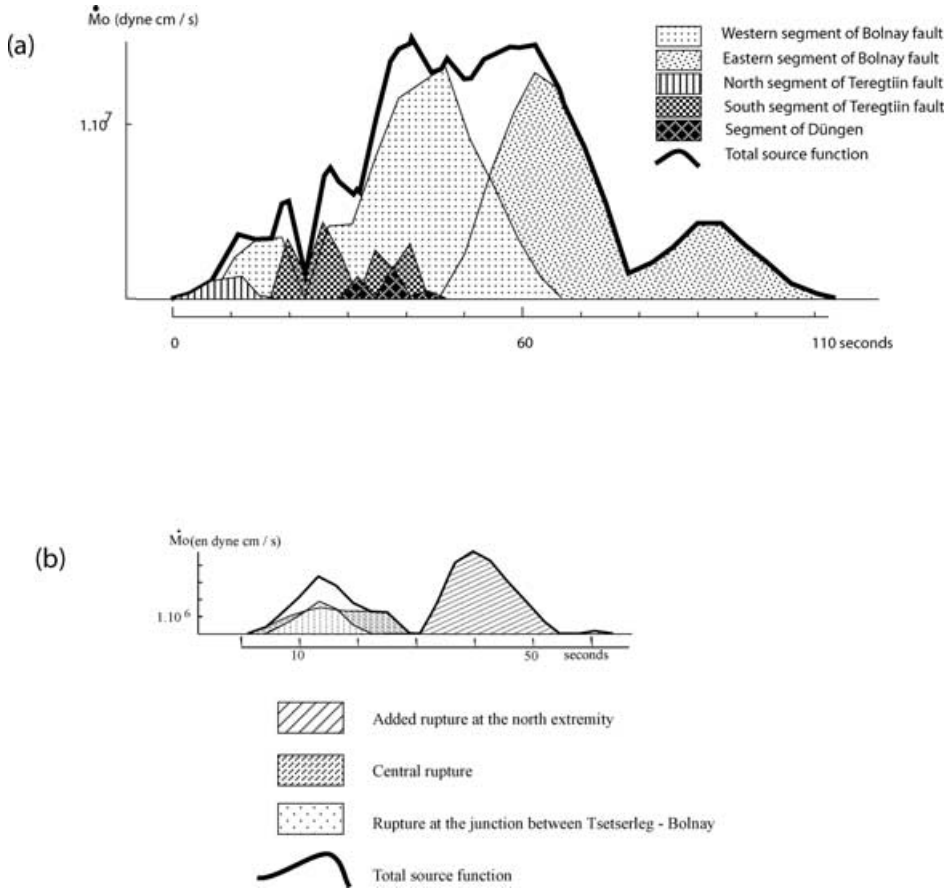

Figure 10. (a) Source function of the Bolnay earthquake. (b) Source function of the Tsetserleg earthquake with an eastward rupture propagation.

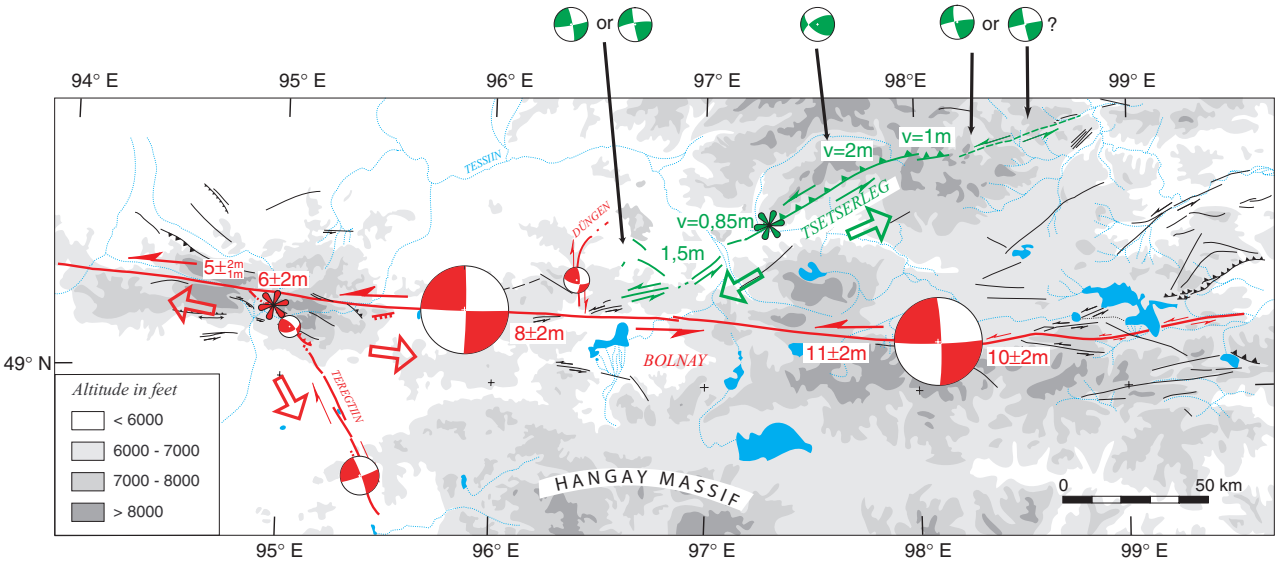

Figure 11. Surface ruptures, epicentre (star), focal mechanism of each segment, and rupture propagation direction (open arrows) for Tsetserleg (green) and Bolnay (red) earthquakes.

DISCUSSION

The minimal depth of the rupture for a large earthquake is equal to the whole thickness of the seismogenic layer. A rupture depth of the 1905 events restrained to a seismogenic layer of 20 km (Baljinnyam *et al.* 1993) seems underestimated in a region where the crust is thickened. If the deformation rate is slow, the region under the seismogenic layer moves with ductile flow, while during an earthquake it becomes brittle. In consequence, it is possible for very large earthquakes to break under the seismogenic zone. Lemiszki & Brown (1988), Blundel (1990), Klemperer & Peddy (1992), Jones *et al.* (1992) and McBride (1995) observed

Table 4. The parameters of the solutions for the Tsetserleg earthquake (1905 July 9).
a: Model with an eastward rupture propagation: Mo total = $1.06 \pm 0.05\ 10^{21}$ N m = > $M_w = 7.95 \pm 0.02$

Depth of nucleation = 15 km	Strike (deg)	Dip (deg)	Slip (deg)	Distance (km)	Azimuth (deg)	Delay (seconds)	Depth of rupture (km)	Mo (N m)	Duration (sec)	Deduced slip (m)
Tsetserleg centre	238.0 NI	64.0 NI	37.0 NI	0	0	0	50.0 NI	(2.54 ± 0.09)e+20	28	2.4
Tsetserleg south	80.0 NI	84.9 ±1.8	7.0 ± 2.0	80 NI	240 NI	3.27 ± 0.27	50.0 NI	(1.77 ± 0.15)e+20	18	2.6
Tsetserleg north	258.0 NI	88.0 NI	3.0 NI	45 NI	240 NI	29.56 ± 0.39	50.0 NI	(6.30 ± 0.25)e+20	24	7.0

b: Model with a westward rupture propagation: Mo total = $9.97 \pm 0.69\ 10^{20}$ N m = > $M_w = 7.94 \pm 0.02$

Depth of nucleation = 15 km	Strike (deg)	Dip (deg)	Slip (deg)	Distance (km)	Azimuth (deg)	Delay (seconds)	Depth of rupture (km)	Mo (N m)	Duration (sec)	Deduced slip (m)
Tsetserleg north	260.0 NI	84.0 NI	13.0 NI	0	0	0	58 ± 1	(2.38 ± 2.20)e+19	12	0.5
Tsetserleg centre	238.0 NI	64.0 NI	37.0 NI	50 NI	240 NI	2.35 ± 2.63	70 ± 1	(3.04 ± 0.23)e+20	36	1.6
Tsetserleg south	260.0 NI	80.0 NI	4.0 NI	100 NI	245 NI	33.38 ± 0.92	52 ± 4	(6.69 ± 0.24)e+20	27	6.3

'NI' indicates that the parameter has not been inverted. The uncertainties on the rupture depth for the model b are low because most of the other parameters where fixed in the inversion.

from seismic profiles that strike-slip faults can cut the Moho.

It is interesting to compare Bolnay earthquake with the Kokoxili earthquake (Kunlun, 2001 November 14, left lateral strike-slip, $M_w = 7.9$) whose nucleation and rupture depth are shallower than 20 km (Rivera *et al.* 2003). However, the Kokoxili ($L = 400$ km), as the San Andreas earthquake of 1906 ($M_w = 7.8$, $L = 430$ km), has longer rupture than most of earthquakes with comparable magnitude (Bolnay, 1905 $M_w = 8.3$, $L = 455$ km, Erzincan 1939 $M_w = 7.9$, $L = 350$ km, Gobi Altay 1957 $M_w = 7.8$, $L = 250$ km) (Rivera *et al.* 2003). But the average slip (6 ± 2 m) during the Kokoxili event is smaller than that of the Bolnay earthquake (8 ± 2 m to 10 ± 2 m). These large values could be related to the straight geometry of the rupture, limiting the barriers and allowing then a propagation of the rupture over an important length. However, the seismic moment of Kokoxili is about 10^{21} N m (with 400 km active fault and slip of about 6 m) when the main segment of Bolnay is at minimum $3.3\ 10^{21}$ N m (with 375 km active fault and slip of about 10 m). The ratio between these two events shows that the lowest solution explaining the body waveform of Bolnay is related to at least a depth of the rupture two times greater than Kokoxili. It would be at least 40 km for Bolnay. This appears to be the minimum depth of the rupture on Bolnay fault.

They are several published empirical relation between length of surface rupture and displacement (Wells & Coppersmith 1994; Scholz 2002). An empirical relation has been proposed where the displacement $u = \alpha L$, with $\alpha = 1.5\ 10^{-5}$ for plate boundaries and $6.5\ 10^{-5}$ for intraplate earthquakes (Scholz *et al.* 1986; Scholz 2002). We have $\alpha \cong 2.6\ 10^{-5}$ in the case of the Bolnay and Gobi-Altay earthquakes (Mongolia, 4 December 1957, Ritz *et al.* 1995), $\alpha \cong 3.4\ 10^{-5}$ in the case of Fu Yun earthquake (Chinese Altay, 1931 August 10) and $\alpha \cong 1.5\ 10^{-5}$ in the case of Kokoxili (Kunlun, 2001 November 14).

Fig. 13 shows the recorded seismicity from 1964 up to 2000 (Adiya *et al.* 2003) in the area of the Tsetserleg and Bolnay earthquakes. We see that, 100 yr after these large events, the activity is still located near these faults. The return periods on the Gobi-Altay segment are between 3000 and 4000 yr (Prentice *et al.* 2002; Ritz *et al.* 2003). Calais *et al.* (2003) estimated a left lateral slip rate of 2.6 ± 1 mm yr^{-1} on the Bolnay fault, using GPS measurements (from 1994 to 2002), giving a return period of 4500 ± 1750 yr. These late events can then be considered as late aftershocks of the 1905 earthquakes (Schlupp 1996).

CONCLUSIONS

Particular effort has been done to retrieve a no deformed signal from the historical seismograms. A continuity of the waveform, during the gap related to the minutes mark, has been obtained using predictive filters. This step must be done precisely before any further analysis of the body waveform.

To constrain the modelling of these earthquakes we used the detailed surface ruptures observations and their distribution between the two events. The rupture propagation velocity is supposed to be 2.5 km s^{-1} for the two events. The nucleation and rupture depths remain uncertain. Three cases have been explored: (1) nucleation and rupture in the seismogenic layer; (2) nucleation in the seismogenic layer with rupture propagation down to the base of the crust and (3) nucleation at the interface between the crust and the upper mantle with rupture propagation under the crust. This last case appears to be the most satisfactory to explain our data.

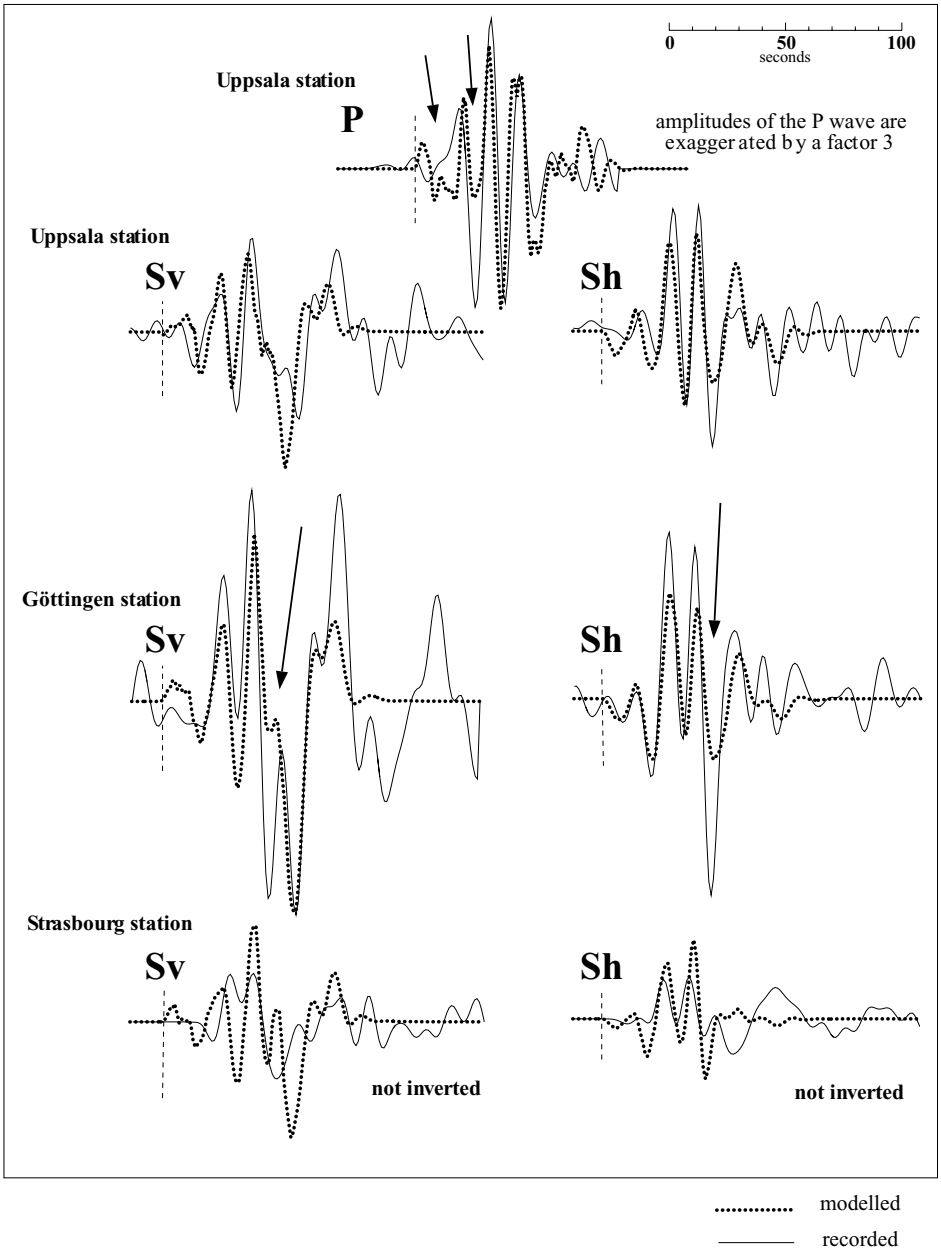

Figure 12. Solutions for an eastward propagation during the Tsetserleg earthquake. Arrows show poorly explained waveforms.

We have good evidence to propose a mainly eastward propagation of the rupture for both 1905 events.

The nucleation of the Tsetserleg earthquake is, for our favoured but not unique solution, at the western extremity of the central segment oriented N60 and characterized by left lateral strike-slip with reverse component. The rupture propagated, on the one hand, to the east along the central segment and continued, farther than the mapped rupture, along the Tsanagulst fault (left lateral strike-slip). On the other hand, it propagated to the west along a N80 structure with left lateral strike-slip until its junction with the Bolnay fault. The seismic moment of the Tsetserleg earthquake is 1.06 ($\pm$0.05) 10^{21} N m with a magnitude $M_w = 8$.

The Bolnay earthquake, 14 days later, starts at the intersection between the main fault (left lateral strike-slip) and the Teregtiin fault (right lateral strike-slip). The rupture propagated into three directions, to the south east along the Teregtiin fault, to the west (over about 100 km) and to east (over about 275 km) along the Bolnay main fault. The Düngen rupture broke about 24 s after the nucleation. For the Bolnay earthquake, the seismic moment vary from 3.97 ($\pm$0.47) 10^{21} to 7.27 ($\pm$0.40) 10^{21} N m functions of the model considered. The magnitude M_w is between 8.34 $\pm$ 0.04 and 8.51 $\pm$ 0.02.

The seismic moment released by the July 23 earthquake is four to seven times greater than that of the 1905 July 9 earthquake. The total duration of the modelled source is 65 s for Tsetserleg and 115 s for Bolnay earthquakes.

A local stress tensor in the Tsetserleg area is proposed from surface ruptures. The stress σ_1 varies from N30, at the south, with a form factor $R = -0.5$ (triaxial compression with σ_1 vertical), to NS, at the north, with a form factor $R = 0$ (uniaxial compression).

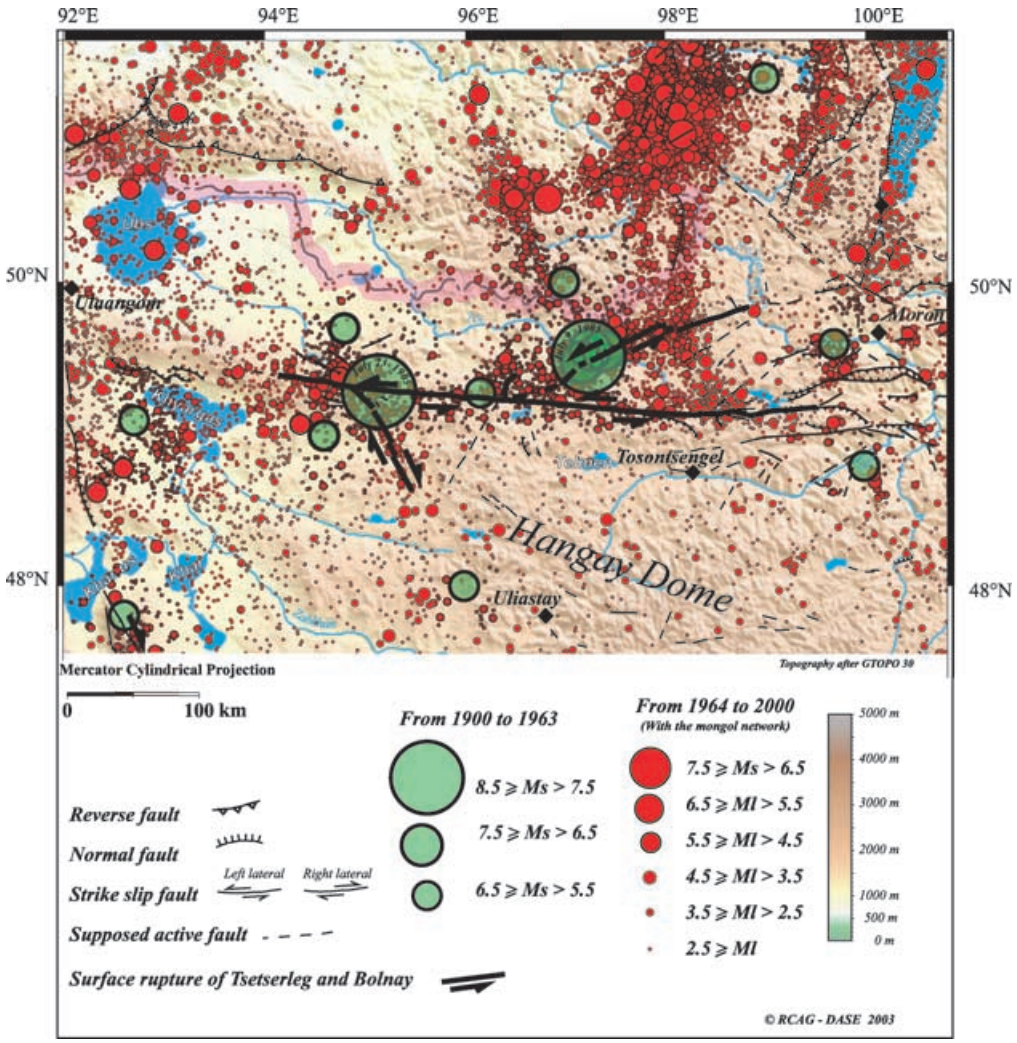

Figure 13. Recorded seismicity in the Bolnay–Tsetserleg region. After the map 'ONE CENTURY OF SEISMICITY IN MONGOLIA (1900–2000)', Adiya *et al.* (2003).

ACKNOWLEDGMENTS

This work has been possible thanks to the archives of the world wide seismic stations. Particular thanks are due to the staff of Jena, Göttingen, Uppsala and Strasbourg stations. We thank our colleagues from the Mongolian Academy of Sciences (Ulaanbaatar), the Mongolian University of Science and Technology (Ulaanbaatar), the Institute of Physics of the Earth, (Moscow) and the Institute of Earth's Crust (Irkutsk) for the facilities we had during the field work. We thank two anonymous reviewers for their careful reading of the manuscript, and their valuable suggestions.

REFERENCES

Abe, K., 1981. Magnitudes of large shallow earthquakes from 1904 to 1980, *Phys. Earth planet. Int.,* **27**, 72–92.

Adiya, M. *et al.*, 2003. One century of seismicity in mongolia (1900–2000), RCAG - DASE, Ulaanbaatar - Bruyeres le Châtel.

Aprodov, V.A., 1960. Seismotectonic observations in the region of the north Hangay earthquake of 1905 (MPR) (in Russian), in Questions of seismotectonics of pre-Baïkal and adjacent territories, *Bull. Soviet Seismol.,* **10,** 90–97.

Armijo, R. & Cisternas, A., 1978. Un problème inverse en microtectonique cassante, *C. R. Acad. Sci. Paris*, **287,** 595–598.

Baljinnyam, I. *et al.*, 1993. *Ruptures of Major Earthquakes and Active Deformation in Mongolia and its Surroundings*, Mem. Geol. Soc. Am., **181,** 64 pp., Boulder Colorado.

Bayasgalan, A., 1999. Active Tectonics of Mongolia, *PhD thesis*, 182 pp. University of Cambridge, Cambridge.

Blundel, D.J., 1990. Seismic images of continental lithosphere, *J. Geol. Soc.,* **147,** 895–913.

Cadek, O., 1987. Studying earthquake ground motion in Prague from Wiechert seismograph records, *Gerl. Beitr. Geoph.,* **96,** 438–447.

Calais, E., Vergnolle, M., San'kov, V., Lukhnev, A., Miroshnitchenko, A., Amarjargal, S. & Déverchère, J., 2003. GPS measurements of crustal deformation in the Baikal-Mongolia area (1994–2002): Implications for current kinematics of Asia, *J. Geophys. Res.,* **108**(B10), 2501, doi:2510.1029/2002JB002373.

Chen, W.-P., 1988. A brief update on the focal depths of intracontinental earthquakes and their correlations with heat flow and tectonic age, *Seism. Res. Lett.,* **59,** 263–272.

Chen, W.P. & Molnar, P., 1983. Focal depths of intracontinental and intraplate earthquakes and their implications for the thermal and mechanical properties of the lithosphere, *J. geophys. Res.,* **80,** 4183–4214.

Crouse, C.B. & Matuschka, T., 1983. Digitization noise and accelerograph pen offset associated with Japanese accelerograms, *Bull. seism. Soc. Am.,* **73,** 1187–1196.

Delouis, B., Déverchère, J., Melnikova, V., Radziminovitch, N., Loncke, L., Larroque, C., Ritz, J.F. & San'kov, V., 2002. A reappraisal of the 1950 (Mw 6.9) Mondy earthquake, Siberia, and its relationship to the strain pattern at the south-western end of the Baikal rift zone, *TerraNova*, **14,** 491–500.

Déverchère, J., Houdry-Lémont, F., Diament, M., Solonenko, N.V. & Solonenko, A.V., 1991. Evidence for a seismogenic upper mantle and lower crust in the Baikal Rift, *Geophys. Res. Lett.,* **18,** 1099–1102.

Déverchère, J., Petit, C., Gileva, N., Radziminovitch, N.V.M. & San'kov, V., 2001. Depth distribution of earthquakes in the Baikal rift system and its implications for the rheology of the lithosphere, *Geophys. J. Int.,* **146,** 714–730.

Ferrari, G., 2000. Multidisciplinary projects to look back on the roots of seismology, *Actes de les V Trobades d'Historia de la Ciència de la Tècnica*, 13–35.

Ilyin, A.V., 1978. Comment on 'The July 9 and 23, 1905, Mongolian earthquakes: a surface wave investigation' by Emile Okal, *Earth planet. Sci. Lett.,* **41,** 107–109.

Jones, A.G., Kurtz, R.D., Boerner, D.E., Craven, J.A., McNeice, G.W., Gough, D.I., DeLaurier, J.M. & Ellis, R.G., 1992. Electromagnetic constraints on strike-slip geometry—The Fraser River fault system, *Geology*, **20,** 561–564.

Kanamori, H., 1977. The Energy Release in Great Earthquakes, *J. geophys. Res.,* **82,** 2981–2987.

Kennett, B.L.N., 1991. *IASPEI 1991 Seismological Tables*, 167 pp., Research School of Earth Sciences, Canberra.

Khil'ko, S.D. *et al.*, 1985. *Earthquakes and the Bases of the Seismic Zoning of Mongolia*, The Joint Soviet–Mongolian Scientific Reasearch Geological Expedition, **41,** 225 pp.

Klemperer, S.L. & Peddy, C., 1992. Seismic reflection profiling and the structure of the continental lithosphere., in *Understanding the Earth*, pp. 251–274, eds Brown, G., Hawkesworth, C. & Wilson, C., Cambridge University Press, Cambridge.

Klinger, Y., Xu, X., Tapponnier, P., Van der Woerd, J., Lasserre, C. & King, G., 2005. High-Resolution Satellite Imagery Mapping of the Surface Rupture and Slip Distribution of the Mw ~7.8, 14 November 2001 Kokoxili Earthquake, Kunlun Fault, Northern Tibet, China. *Bull. seism. Soc. Am.,* **95,** 1970–1987.

Lemiszki, P.J. & Brown, L.D., 1988. Variable crustal structure of strike-slip fault zones as observed on deep seismic reflection profiles, *Geol. Soc. Am. Bull.,* **100,** 665–676.

Mainka, C., 1910. Seismometrsche Beobachtungen in Strassburgi. E. in der Zeit von 1. Januar bis 31. Dezember 1905, *Beiträge für Geophysik*, **X,** 387–467.

McBride, J.H., 1995. Does the Great Glen fault really disrupt Moho and upper mantle structure?, *Tectonics*, **14,** 422–434.

Michelini, A., De Simoni, B., Amato, A. & Boschi, E., 2005. Collection, Digitization and Distribution of Historical Seismological Data at INGV, *EOS TRANSACTIONS AGU, 12 July 2005*, **86,** 28.

Nabelek, J., 1984. *Determination of Earthquake Source Parameters from Inversion of Body Waves*, Massachusetts Institute of Technology, Cambridge.

Nelson, M.R., McCaffrey, R. & Molnar, P., 1987. Source parameters for 11 earthquakes in the Tien Shan, central Asia, determined by *P* an *SH* Waveform inversion, *J. geophys. Res.,* **92,** 12 629–12 648.

Okal, E., 1977. The July 9 and 23, 1905, Mongolian earthquakes: a surface wave investigation, *Earth planet. Sci. Lett.,* **34,** 326–331.

Petit, C., Déverchère, J., Calais, E., San'kov, V. & Fairhead, D., 2002. Deep structure and mechanical behavior of the lithosphere in the Hangai-Hövsgöl region, Mongolia: new constraints from gravity modelling, *Earth planet. Sci. Lett.,* **197,** 133–149.

Pintore, S., Quintiliani, M. & Franceschi, D., 2005. Teseo: A vectoriser of historical seismograms, *Comput. Geosci.,* **31**(10), 1277–1285.

Prentice, C.S., Kendrick, K.J., Berryman, K., Bayasgalan, A., Ritz, J.F. & Spencer, J.Q., 2002. Prehistoric ruptures of the Gurvan Bulag fault, Gobi Altay, Mongolia, *J. geophys. Res.,* **107**(B12), 2321, doi:2310.1029/2001JB000803.

Press, W.H., Teukolsky, S.A., Vetterling, W.T. & Flannery, B.P., 1992. *Numerical Recipes in FORTRAN: The Art of Scientific Computing*, Cambridge University Press, Cambridge.

Reid, H.F., 1910. *The Mechanics of the Earthquake, The California Earthquake of April 18, 1906*, 192 pp., Carnegie Institution of Washington, Washington, D.C.

Reid, H.F., 1925. The influence of friction on seismographs, *Bull. seism. Soc. Am.,* **15,** 222–241.

Richter, C.F., 1958. *Elementary Seismology*, Freeman, W.H. Co., San Francisco.

Ritz, J.F., Brown, E.T., Bourlès, D.L., Philip, H., Schlupp, A., Raisbeck, G.M., Yiou, F. & Enkhtuvshin, B., 1995. Slip rates along active faults estimated with cosmic-ray-exposure dates: application to the Bogd fault, Gobi-Altaï, Mongolia, *Geology*, **23,** 1019–1022.

Ritz, J.-F. *et al.*, 2003. Late Pleistocene to Holocene slip rates for the Gurvan Bulag thrust fault (Gobi-Altay, Mongolia) estimated with 10Be dates, *J. geophys. Res.,* **108**(B3), 2162, doi:2110.1029/2001JB000553.

Rivera, L., Van der Woerd, J., Tocheport, A., Klinger, Y. & Lassere, C., 2003. The Kokoxili, November 14, 2001, earthquake: history and geometry of the rupture from teleseismic data and field observation, paper presented at European Geophysical Society, Geophysical Research Abstracts, Nice.

Schlupp, A., 1996. Néotectonique de la Mongolie Occidentale analysée à partir de données de terrain, sismologiques et satellitaires, *PhD thesis*, 270 pp, ULP, Strasbourg.

Scholz, C.H., 2002. *The Mechanics of Earthquakes and Faulting*, 471 pp., Cambridge University Press, Cambridge.

Scholz, C.H., Aviles, C.A. & Wesnousky, S.G., 1986. Scaling differences between large interplate and intraplate earthquakes, *Bull. seism. Soc. Am.,* **76,** 65–70.

Villaseñor, A., Ritzwoller, M.H., Levshin, A.L., Barmin, M.P., Engdahl, E.R., Spakman, W. & Trampert, J., 2001. Shear velocity structure of central Eurasia from, inversion of surface wave velocities, *Phys. Earth planet. Inter.,* **123,** 169–184.

Voznesenskii, A.V., 1962. *Investigation of the region of the Hangay earthquakes of 1905 in northern Mongolia (en Russe). Materials from the department of Physical Geographical Society of the USSR*, 50 pp., Leningrad.

Voznesenskii, A.V. & Dorogostaiskii, V.C., 1914. Map of the earthquakes of 9 and 23 July, 1905 (scale1/420 000) SPb.

Wells, D.L. & Coppersmith, K.J., 1994. New empirical relationships among magnitude, rupture length, rupture width, rupture area, and surface displacement, *Bull. seism. Soc. Am.,* **84,** 974–1002.

Wiechert, E., 1903. *Theorie der automatischen Seismographen. Der Königlichen Gesellschaft der Wissenschaften zu Göttingen.*, 128, Weidmannsche Buchhandlung, Berlin.

Wiechert, E., 1904. Ein astatisches Pendel hoher Empfindlichkeit zur mechanischen Registrierung von Erdbeben, *Beit. Geoph., VI*, 435–450.

Wood, H.O., 1921. A list of the seismological stations of the world, *Bull.e Natl. Res. Council*, **2,** 397–538.

Zorin, Y.A., Mordvinova, V.V., Turutanov, E.K., Belichenko, B.G., Artemyev, A.A., Kosarev, G.L. & Gao, S.S., 2002. Low seismic velocity layers in the Earth's crust beneath Eastern, Siberia (Russia) and Central Mongolia: receiver function data, and their possible geological implication, *Tectonophysics*, **359,** 307–327.